Original Article OPEN ACCESS

Simulation-Based Insights into Light Soaking and Light-Induced Degradation in Perovskite Solar Cells

Guillem Álvarez Pérez[1,2], Karim Medjoubi[1], Arthur Julien[3], Jean Baptiste Puel[1,4], and Jean François Guillemoles[1,2]
[1] Institut Photovoltaïque d'Île-de-France (IPVF), Palaiseau, 91120, France
[2] Institut Photovoltaïque d'Île-de-France (IPVF), UMR 9006, CNRS, École Polytechnique, IP Paris, Chimie Paristech, PSL, Palaiseau, 91120, France
[3] School of Photovoltaic and Renewable Energy Engineering, University of New South Wales, Sydney, NSW 2052, Australia
[4] EDF R&D, Palaiseau, 91120, France

Supplementary material

Details about device fabrication

All devices analysed in this work share the same device architecture and were fabricated using the same overall process flow. The only variations between split groups concern the perovskite precursor preparation conditions, namely the timing of solution preparation relative to deposition and whether the precursor solution was preheated prior to deposition. These two variables define the four split groups summarized in *Table S1*. Apart from these differences, all other fabrication steps, including substrate preparation, ETL, HTL, perovskite, and top-electrode deposition procedure were kept identical across devices.

The devices consisted of an NIP architecture. They were fabricated on glass substrates with fluorine-doped tin oxide (FTO) as the bottom electrode, compact titanium dioxide (TiO_2) and mesoporous titanium dioxide (mp-TiO_2) as the ETL, a triple-cation perovskite as the absorber layer, poly(triarylamine) (PTAA) as the HTL, and gold as the back electrode. Compact TiO_2 thin films were prepared by Atomic Layer Deposition (ALD) in a BENEQ TFS-200 reactor. Titanium (IV) i-propoxide ($Ti(OiPr)_4$, TTIP, min. 98%, STREM) and deionized water were used as Ti and O sources, respectively. Afterwards, the mp-TiO_2 layer was deposited in ambient atmosphere by spin-coating of a TiO_2 paste solution in ethanol (1:7 weight ratio) at a speed of 4000 rpm for 30 s, followed by annealing on a hot plate for 45 min with several temperature steps up to 500 °C. Following the ETL preparation, perovskite and HTL layer preparation and deposition were performed inside a nitrogen glovebox. The triple-cation perovskite, $Cs_{0.05}(MA_{0.167}FA_{0.833})_{0.95}Pb(I_{0.842}Br_{0.158})_3$, was prepared by mixing PbI_2, $PbBr_2$, FAI, MABr, and CsI in DMF:DMSO (4:1; v:v). $Pb(SCN)_2$ was used as dopant and dissolved in the ink at a ratio of 1%. The ink was deposited by spin-coating and dynamically quenched using chlorobenzene. The perovskite-coated substrate was immediately annealed at 100 °C for 30 min. Afterwards, the HTL solution, consisting of 10 mg of PTAA, 3.75 µL of tBP, and 2.4 µL of Li-TFSi solution (1.8 M stock solution in acetonitrile) per 1 mL of toluene, was spin-coated onto the perovskite thin films. Gold (100 nm) was thermally evaporated under high vacuum through a shadow mask to define an active area of 0.2 cm^2.

Device ID	Solution timing	Preheating (70 °C, 1 h)	Included	Notes
Cell 1.1	D0 (day of deposition)	No	No	Excluded (erratic behaviour)
Cell 1.2	D0 (day of deposition)	No	Yes	-
Cell 2.1	D0 (day of deposition)	Yes	No	Excluded (early failure)
Cell 2.2	D0 (day of deposition)	Yes	No	Excluded (early failure)
Cell 3.1	D-1 (one day before deposition)	No	Yes	-
Cell 3.2	D-1 (one day before deposition)	No	Yes	-
Cell 4.1	D-1 (one day before deposition)	Yes	Yes	-
Cell 4.2	D-1 (one day before deposition)	Yes	Yes	-

Table S1. Device affiliation to split groups and inclusion in the analysis. Groups are defined by perovskite precursor preparation: solution timing (D0: prepared the same day; D-1: prepared one day in advance) and preheating prior to deposition (70 °C for 1 h vs none). Devices excluded from the analysis due to early failure or erratic measurement behaviour are identified in the table.

Detail on processing of experimental data

The experimental data analysed tracks the temporal evolution of optoelectronic parameters during ageing. Processing is implemented to reduce noise in the raw data while preserving relevant physical information. Hereafter the process conducted to process data is introduced. Initially, a Savitzky-Golay filter is applied to the JV curves recorded in both forward and reverse scan directions, smoothing them along the voltage range. Afterward, parameters are extracted, and outliers are removed based on criteria for low V_{OC}, FF, and the R_{SH}/R_S ratio. Time derivatives of the parameters are also inspected, and data with abrupt, unphysical variations is discarded. Finally, a moving median filter is used to smooth JV curves over time.

After processing both scan directions, their average is taken to capture the overall cell behaviour and get rid of capacitive effects. LS and LID intervals are then selected by direct observation of the experimental data, ensuring that all electrical parameters evolve simultaneously following performance increase or decline. In addition, time spans are selected where power changes linearly, based on the assumption that the underlying physical mechanisms in these periods are simpler to analyse compared to more complex, coupled trends where multiple factors may be influencing the solar cell's response simultaneously.

Inputs for the simulations

The model employed simulates one-dimensional solar cells consisting of three active layers: a perovskite absorber positioned between the HTL and the ETL. These layers are assumed to have uniform properties with parallel interfaces. Various material parameters, such as layer thickness, bandgap, and relative permittivity, can be adjusted to reflect the specific characteristics of the device being studied, which are listed as follows.

Parameter	**Value**	**Parameter**	**Value**
Perovskite thickness (nm)	500	Acceptor density in ETL (cm^{-3})	0
Perovskite bandgap (eV)	1.619	Donor density in ETL (cm^{-3})	$\in [10^{18}, 10^{19}]$
Perovskite electron affinity (eV)	3.9	Electron mobility in ETL ($cm^2\ V^{-1}\ s^{-1}$)	$\in [5\ 10^{-3}, 5\ 10^{-1}]$
Perovskite relative permittivity	64	Hole mobility in ETL ($cm^2\ V^{-1}\ s^{-1}$)	$5\ 10^{-2}$
Perovskite CB effective density of states (cm^{-3})	10^{19}	HTL thickness (nm)	50
Perovskite VB effective density of states (cm^{-3})	10^{19}	HTL bandgap (eV)	3.2
Deep defects in the perovskite (cm^{-3})	$\in [10^{14}, 10^{17}]$	HTL relative permittivity	3.5
Electron mobility in perovskite ($cm^2\ V^{-1}\ s^{-1}$)	$\in [5\ 10^{-2}, 10]$	HTL electron affinity (eV)	2.22
Hole mobility in perovskite ($cm^2\ V^{-1}\ s^{-1}$)	$\in [5\ 10^{-2}, 10]$	HTL CB effective density of states (cm^{-3})	$2\ 10^{18}$
Perovskite/ETL interface defects (cm^{-2})	$\in [10^{14}, 10^{17}]$	HTL VB effective density of states (cm^{-3})	$2\ 10^{18}$
Perovskite/HTL interface defects (cm^{-2})	$\in [10^{14}, 10^{17}]$	Acceptor density in HTL (cm^{-3})	$\in [2\ 10^{17}, 2\ 10^{18}]$
ETL thickness (nm)	50	Donor density in HTL (cm^{-3})	0

ETL Bandgap (eV)	3.2	Hole mobility in HTL ($cm^2\ V^{-1}\ s^{-1}$)	$\in [5\ 10^{-3}, 5\ 10^{-1}]$
ETL Relative permittivity	9	Electron mobility in HTL ($cm^2\ V^{-1}\ s^{-1}$)	$5\ 10^{-2}$
ETL electron affinity (eV)	3.9	External series resistance ($\Omega\ cm^2$)	$\in [10^{-1}, 20]$
ETL CB effective density of states (cm^{-3})	10^{19}	External shunt resistance ($\Omega\ cm^2$)	$\in [2\ 10^2, 10^3]$
ETL VB effective density of states (cm^{-3})	10^{19}		

Table S2. Parameter inputs used for simulations of the devices studied. Fixed values have been obtained from experimental measures or the literature ([13] - [18]), while material parameter ranges present the values explored for LS and LID mechanisms. ETL and HTL stand for electron and hole transport layer, CB and VB for conduction and valence band, respectively.

Parameter identifiability from GA ensembles

After GA selection, the retained parameter sets reproduce the experimental JV metrics within the prescribed tolerance. The post-selection distributions provide qualitative information on how strongly each parameter is constrained by JV data under the chosen bounds and device structure. In some cases, the selected values concentrate around a dominant peak, indicating a relatively constrained range. In other cases, the distributions exhibit several peaks (often spread over a wide range), showing that multiple distinct parameter ranges can reproduce the experimental JV within tolerance. In such cases the parameter is less tightly constrained by JV data alone. *Figure S1* provides an illustrative example of this multi-peak behaviour, in contrast with the distribution showing a dominant peak in *Figure 5c.*

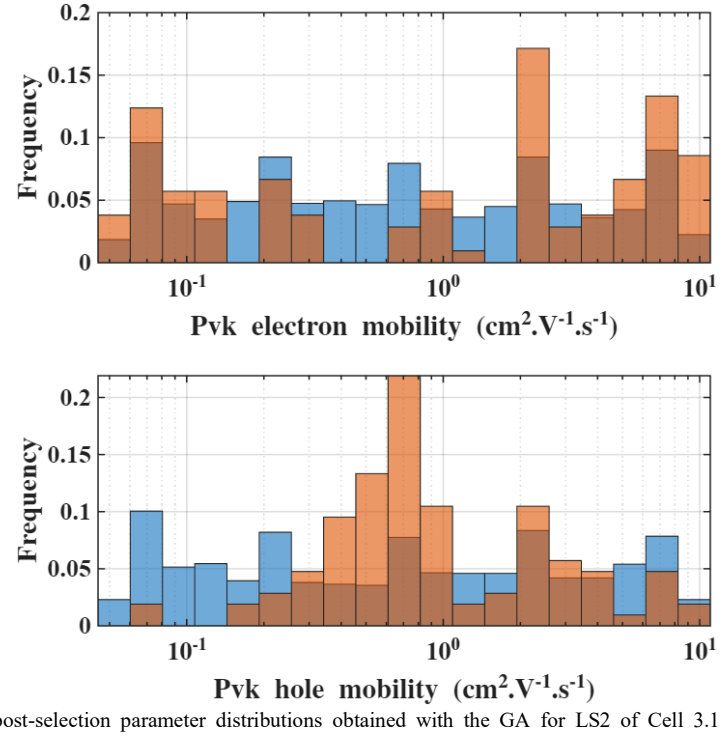

Figure S1. Example of multi-peak post-selection parameter distributions obtained with the GA for LS2 of Cell 3.1. Histograms comparing the initial population (blue) with the retained solutions after selection (orange) for perovskite electron mobility (top) and hole mobility (bottom). The selected distributions exhibit several peaks, indicating that multiple distinct parameter ranges can reproduce the experimental JV metrics within the prescribed tolerance. In such cases, the parameter is less tightly constrained by JV data alone than for parameters showing a single dominant peak.